JOURNAL OF MATERIALS SCIENCE 14 (1979) 1326–1338

The thermal conductivity of carbon fibre-reinforced composites

M. W. PILLING*, B. YATES, M. A. BLACK
Department of Pure and Applied Physics, University of Salford, Salford, UK

P. TATTERSALL
Fothergill and Harvey Ltd, Littleborough, Lancashire, UK

Measurements of the thermal conductivity between approximately 80 and 270 K of a series of unidirectional and bidirectional specimens of epoxy resin DX210/$BF_3$400 reinforced with Morganite high modulus (HMS) and high strength (HTS) carbon fibres are reported for in-plane and out-of-plane directions. The main features of the results conform with expectations based upon known structural properties of the fibres and predictions based upon current theoretical models. Employing the results for the composites in association with results for the pure resin, the account concludes with an assessment of some of the heat transmission characteristics of the fibres.

1. Introduction

A recognition of the importance of the high stiffness and strength weight ratios of carbon fibre-reinforced plastics (CFRP) has led to extensive investigations of their mechanical properties and associated effects of environmental degradation (e.g. [1–4]). More recently, an appreciation of the influence of temperature change has led to investigations of the thermal expansion characteristics of various CFRP laminae and laminates [5, 6]. One outcome of these investigations has been that features of the behaviour of CFRP structures operating under realistic working conditions can now be assessed with a reasonable degree of confidence.

The dissipation of heat by these materials is a further subject of some importance, but the shortage of experimental thermal conductivity data has so far prevented a comprehensive appraisal of their heat transmission characteristics. The investigation to be described was undertaken against this background, the object being to provide characterization data for immediate technological application, which might also be employed for assessing the standing of current theoretical models of heat conduction in composite solids.

2. The specimens

2.1. Constituent materials

For the purpose of the present investigation attention was concentrated upon one resin system and two types of carbon fibre. The resin was DX210, the hardener $BF_3$400, both of which were produced by Shell Chemicals Ltd. The type I (HMS) and type II (HTS) carbon fibres employed were both manufactured by Morganite Modmor Ltd from polyacrilonitrile precursor.

2.2. Pure resin

Specimens of the pure resin were required in the form of circular discs, 35 mm diameter. These were cut from a cylinder which was cast in a rubber mould having this internal diameter. The procedure adopted was to add the appropriate amount of hardener to a quantity of 80% resin in a solution of methylethylketone and to place the resulting mixture in a vacuum oven at 100° C together with the mould, the inside of which had first been sprayed with a silicone release agent. The oven was pumped for approximately 10 min, until the resin had ceased to bubble. After venting the oven the resin was poured into the mould where it was pumped again until bubbling ceased, following which the oven was again vented to the

*Present address: Chloride Technical Ltd, Manchester, UK.

atmosphere and the curing of the resin was allowed to proceed for 1 h, during which it hardened. The resin cylinder was then removed from the mould and cooled. Upon being found to be void-free and glass-clear its temperature was finally raised to 150° C, at which it was held for 2 h in order to complete the curing cycle.

2.3. Composite bars

The composite bars were assembled from sheets of fibre pre-impregnated with resin (pre-preg). Having decided upon the fibre volume fraction required in a bar, the required volume of 40% resin in solution was calculated. This figure was then increased by 25% in order to allow for losses and to ensure a good resin flow during the final moulding process. This was poured evenly over the fibre tows, which were laid on a non-stick surface of siliconized paper. After manipulation, suitably wetted tows were selected and laid parallel to and equidistant from one another on another sheet of siliconized paper. A further sheet of siliconized paper was laid on top and the sandwich was transferred to a hot plate, where it was rolled to remove trapped air and to produce a more nearly uniform distribution of fibres. The top sheet of siliconized paper was removed and the pre-preg was heated at 80° C for 2 min in order to achieve a partial cure and to drive off most of the solvent. It was then removed from the oven, cooled, the top sheet of siliconized paper was replaced and the pre-preg sheet was returned to the hot plate, where it was rolled again. This process was repeated until the pre-preg was firm, tacky and contained a uniform dispersion of fibres, following which it was stored in a freezing cabinet until required.

For thermal conductivity measurements in a direction parallel to the fibres bar specimens were required, while for measurements perpendicular to the fibres plates were required. The leaky mould technique was employed in the production of both sets of specimens. The temperature of the assembly was raised to 170° C under high pressure, following which the composite block was removed from the mould, which was then sprayed with release fluid for a second time before the block was replaced and cured under closing pressure for 1 h at 170° C. The pressure was controlled by stops which defined the final lateral specimen dimensions. The block was then removed from the mould and cured for a further hour at 170° C.

Great care was taken in accurately aligning the constituent laminae of the different composite blocks before these were assembled in the moulds. Precautions were also taken to standardize the fibre types, as far as this was possible, and all the HMS fibre employed in the investigation came from the same batch. In the case of the HTS fibre practical problems necessitated the fibre required for the ±45° bar being taken from a different batch from that employed in the unidirectional and 0° −90° bar.

2.4. Specimen preparation

All dimensions of the bar specimens were intentionally oversize. Approximately 7 mm was cut from the end of each bar with a slicing wheel and the remaining faces were reduced appropriately with the aid of a surface grinder until the dimensions had been reduced to 100 mm x 6 mm x 6 mm, by which time the fibre lay-up was properly balanced in the cases of the cross-plies. These dimensional reductions were undertaken very slowly and the bar temperature was monitored in order to ensure that there was no overheating, which might have affected the physical characteristics of the bars. Disc-shaped specimens, approximately 40 mm diameter, were produced from the moulded plates with the aid of a disc cutter. The diameters were reduced to 35 mm and the thickness of each disc was reduced to the values required by grinding and polishing. A similar procedure was adopted when adjusting the thicknesses of the specimens of pure resin.

Final determinations of fibre volume fraction were effected by density determinations, employed in association with acid digestion. In the case of the bars, tests for voids were applied by the microscopic examination of polished surfaces of specimens, whereas in the case of the plates ultrasonic c-scan techniques were employed. Following these tests, attempts were made to use void-free regions for specimen preparation, as far as this was possible. A list of the specimens prepared and investigated is summarized in Table I.

3. Experimental details

3.1. The apparatus

The main features of the original apparatus have been described in detail by German [7]. Modifications were necessary in order to adapt the system so as to be able to accommodate and investigate the bar specimens, which had fairly high conductivities, and the plate specimens, the

TABLE I The specimens

Specimen designation	Fibre type	Angle between fibre directions (deg)	Direction of thermal conductivity measurements	Fibre volume (%)	Void content (%)
1	No fibres			0.0	Visually assessed to be negligible
2	HMS	0	Parallel to fibres	60.7	0.1
3	HMS	0	Perpendicular to fibres	57.9	0.3
4	HMS	90	Parallel to one set of fibres	55.7	0.8
5	HMS	90	Bisecting angle between fibres	56.1	0.0
6	HTS	0	Parallel to fibres	58.4	2.3
7	HTS	0	Perpendicular to fibres	45.9	0.0
8	HTS	0	Perpendicular to fibres	59.1	0.3
9	HTS	0	Perpendicular to fibres	71.9	0.0
10	HTS	90	Parallel to one set of fibres	62.1	1.2
11	HTS	90	Bisecting angle between fibres	59.3	2.8

thermal conductivities of which were much lower. For the sake of completeness both of the alternative modifications employed to accommodate the specimens will be described briefly.

3.1.1. Searle's bar system

The modification employed for investigating the higher conductivity bar-shaped specimens took the form of a Searle's bar system. The cryostat assembly, which was suspended from the top cap of a Dewar vessel by three stainless steel tubes, is illustrated in Fig. 1. It consisted of a copper specimen chamber, C, surrounded by an outer brass can, B. The specimen, S, was positioned axially in a holder which was located at the centre of the base of the specimen chamber. It was surmounted by a copper heater block, H, and surrounded by a stainless steel radiation shield, R, which terminated in a copper top cap, T, carrying a thermal anchoring post, A, for the electrical leads. Two copper specimen mounting blocks were fabricated. One of these had a circular hole and was used to hold an electrolytic iron reference bar; the other had a square hole and was used to hold the CFRP bar specimens. Good thermal contact between the various demountable components was achieved with the aid of Apiezon vacuum grease. A copper block U was hard soldered to the base of the specimen chamber in order to provide a housing for a platinum resistance thermometer which was used as the sensing element of the specimen chamber temperature controller.

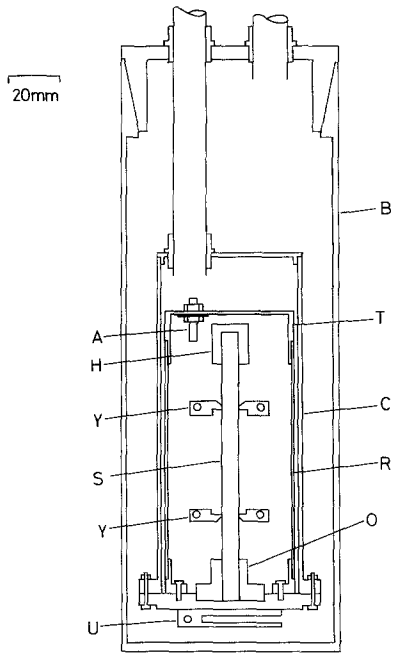

Figure 1 Cryostat assembly for the Searle's bar system. S, specimen; Y, platinum resistance thermometer yokes; H, specimen heating coil; O, specimen mounting block; U, platinum resistance temperature sensor; T, top cap of radiation shield R; A, thermal anchoring post; C, specimen chamber; B, outer can.

A system of pumping tubes allowed the specimen chamber and outer can to be evacuated and further tubes provided entry for the various electrical leads. The specimen chamber was sealed to the bottom plate by "Loctite Stud Lock", which provided convenient access when changing specimens. With liquid nitrogen in the Dewar vessel, mean specimen temperatures between approximately 80 and 270 K could be achieved by passing current through a series of five heating coils which were wound on the outside of the specimen chamber, C, while the enclosures within B were under high vacuum. Temperatures could be held steady within a few millidegrees with the aid of the sensor located in U, which formed one arm

of an a.c. Wheatstone bridge. The out-of-balance signal from the bridge ultimately activated the controller of current supplied to the specimen chamber heating coils. In order to make a measurement, current was passed through the specimen heating coil, H, and the temperature gradient established along the specimen was measured with the aid of platinum resistance thermometers located within the copper yokes, Y. The yokes were bolted to the specimen with which they made contact through blunted knife edges. It was necessary to ensure that the temperature gradient along the radiation shield, R, was identical to that along the specimen. This was achieved at its lower end by thermally anchoring the base of the shield to the specimen holder, while at the upper end, the out-of-balance signal from a differential thermocouple between the heater block, H, and the top cap, T, of the radiation shield activated the supply of current to a heating coil wound on the top section of the radiation shield.

3.1.2. Lees' disc system

For the investigation of the lower conductivity disc-shaped specimens, a Lees' disc arrangement was adopted. This is illustrated in Fig. 2, in which the outer brass can, B, the specimen chamber, C, and the temperature sensor at U are the same as before. The specimen disc, S, was sandwiched between two copper blocks, which contained the platinum resistance thermometers. The upper block terminated in a pillar, H, on which was wound a heater. The lower block, L, fitted into the base of the specimen chamber and good thermal contact between the various surfaces was achieved with the aid of low vapour pressure greases, "Nonaq" grease being used between the copper blocks and the specimen because of its relatively low viscosity at reduced temperatures. The radiation shield, R, consisted of three sections, the upper and lower members of which were constructed from copper. A nylon insert, N, corresponded in length and position with the specimen, and temperature equality between the upper section of the shield and the upper sandwich block was achieved with the aid of a differential thermocouple which activated a heater wound on the upper section of the shield. The electrical leads to the specimen heater, H, were thermally anchored to the pin, A, and temperature equality between the lower section of the shield and the block supporting the specimen was achieved by thermally connecting these through the base of the specimen chamber.

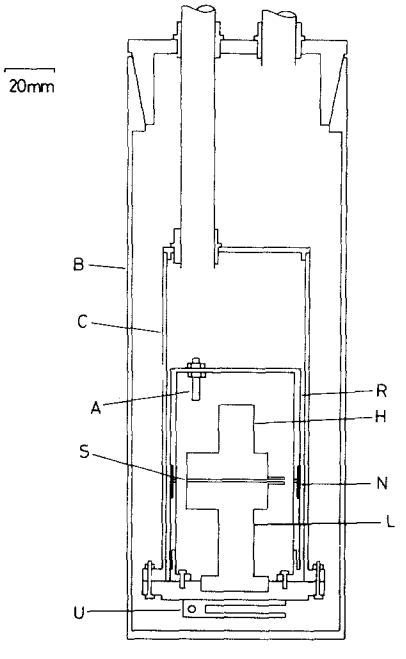

Figure 2 Cryostat assembly for the Lees' disc system. S, specimen; H, specimen heating block; U, platinum resistance temperature sensor; R, radiation shield; N, nylon ring; A, thermal anchoring post; L, specimen support block; C, specimen chamber; B, outer can.

3.2. Performance of the apparatus

By way of assessing the accuracy with which both forms of the apparatus would reproduce established results for well-defined substances, the investigation was preceded by a preparatory proving programme.

In the case of the Searle's bar system the test substance employed was a rod of electrolytic iron, SRM 734, obtained from the National Bureau of Standards. A comparison of the present primary data with the smoothed NBS data [8], illustrated in Fig. 3, reveals agreement within the combined experimental uncertainties at all temperatures.

In the case of the Lees' disc system, vitreous silica was adopted as the test substance. The thermal conductivity of this material has been investigated by a number of workers, employing samples drawn from a variety of sources. The most meaningful comparison involving the present results can probably best be made with the measurements reported by Ratcliffe [9] at the National Physical Laboratory, whose specimen of Vitreosil came from the same supplier as the present specimens, Thermal Syndicate Ltd. From

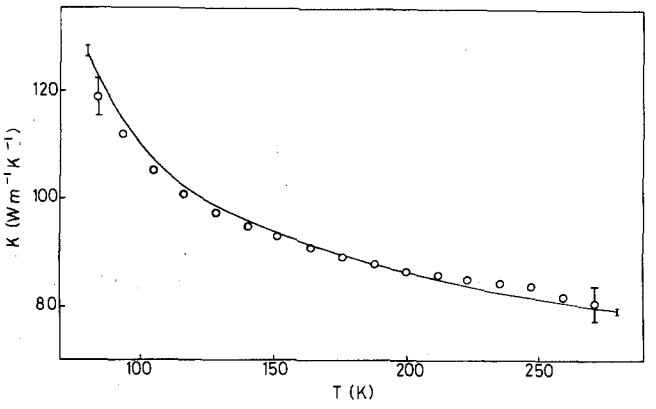

Figure 3 The thermal conductivity K of electrolytic iron, (SRM 734 from the National Bureau of Standards), in which the vertical lines indicate the estimated uncertainty limits: ϕ present primary data; ⊢⊣ smoothed NBS data [8].

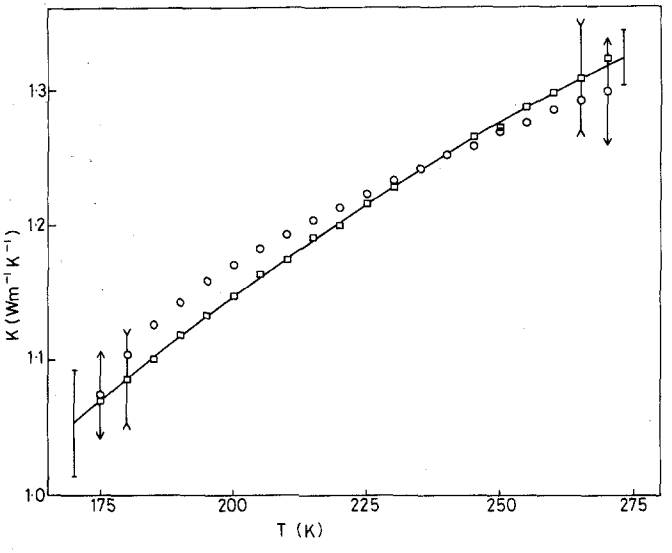

Figure 4 The thermal conductivity K of vitreous silica, in which the vertical lines indicate the estimated uncertainty limits: ϕ, ϕ present primary data employing Rosemount and Minco thermometers respectively; ⊢⊣ smoothed NPL data [9].

the comparison illustrated in Fig. 4 it may be seen that the two sets of results agree within the combined experimental uncertainties at all temperatures.

Platinum resistance thermometers from two sources were employed during the course of the work, all of which were calibrated by Cryogenic Calibrations Ltd. In the earlier part of the investigation, thermometers supplied by the Rosemount Engineering Co Ltd were employed in the investigation of all the bar specimens, including the electrolytic iron reference specimen. With the exception of specimens 3, for which Rosemount Thermometers were used, all the disc specimens were investigated using thermometers produced by Minco Products Inc and supplied by Cryogenic Calibrations Ltd. For this reason the proving programme undertaken with vitreous silica included the use of thermometers drawn from both sources, the results of measurements employing which are illustrated in Fig. 4.

4. Results

4.1. Preliminary considerations

For convenience of analysis the thermal conductivities of the specimens are summarized in smoothed form in Table II. These values were read from smooth lines drawn by eye through plots of the primary experimental data.

In the case of the results taken with the Searle's bar system, after confirming that the apparatus was producing reproducible results from one occasion to another, the accuracy to which the effective separation of the thermometers could be measured was examined by altering the separation of the thermometer yokes and repeating measurements during a completely separate run. An additional precaution was applied by testing for any possible influence of the method of specimen preparation upon the uniformity of temperature through a plane at right angles to the direction of heat flow. This was done by releasing the bolts securing the thermometer yokes to a specimen,

TABLE II Smoothed values of the thermal conductivity K of the specimens described in Table I

T	K (W m^{-1} K^{-1}) for the specimens numbered below										
(K)	1	2	3	4	5	6	7	8	9	10	11
80				(3.30)	(3.64)	(1.55)				(0.94)	(1.02)
90		9.4		4.30	4.61	1.90				1.20	1.24
100		12.0		5.30	5.64	2.27				1.45	1.46
110		14.6		6.35	6.69	2.65				1.70	1.70
120		17.2		7.40	7.75	3.05				1.95	1.94
130		19.7		8.50	8.80	3.43				2.20	2.18
140		22.2		9.66	9.89	3.84				2.45	2.45
150		24.6		10.9	11.0	4.25				2.70	2.71
160		27.1		12.0	12.0	4.66				2.95	2.99
170		29.5		13.1	13.1	5.08				3.20	3.28
175	0.194	30.7	1.194	13.6	13.6	5.29	0.457	0.506	0.746	3.33	3.42
180	0.196	32.0	1.219	14.1	14.1	5.50	0.463	0.523	0.764	3.46	3.56
190	0.198	34.4	1.289	15.1	15.2	5.93	0.473	0.553	0.793	3.71	3.87
200	0.201	36.6	1.331	16.1	16.2	6.35	0.485	0.575	0.829	3.96	4.17
210	0.204	38.9	1.378	17.1	17.1	6.77	0.499	0.598	0.874	4.21	4.48
220	0.207	41.1	1.413	18.0	18.0	7.20	0.514	0.623	0.926	4.46	4.79
230	0.210	43.2	1.423	18.9	18.9	7.62	0.530	0.649	0.968	4.71	5.10
240	0.214	45.2	1.403	19.8	19.7	8.05	0.551	0.676	1.010	4.46	5.42
250	0.218	47.1	1.410	20.7	20.6	8.48	0.574	0.701	1.048	5.21	5.75
260	0.222	48.9	1.447	21.7	21.3	8.90	0.593	0.726	1.089	5.47	6.06
270	0.226	50.6	1.463	22.6	22.0	9.33	0.607	0.747	1.133	5.73	6.39

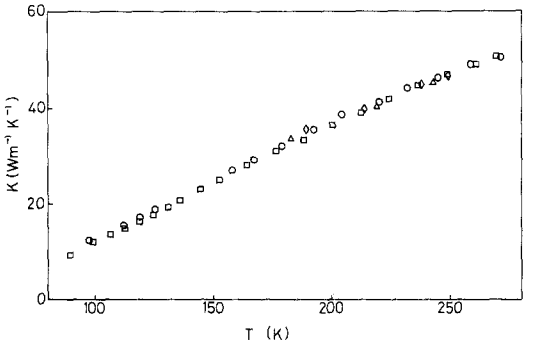

Figure 5 The thermal conductivity K of specimen 2: ○ run 1 (thermometer separation 1); □ run 2 (thermometer separation 1); △ run 3 (thermometer separation 2); ◇ run 4 (thermometer yokes clamped to the other pair of opposite faces, at separation 3).

turning the specimen through 90°, tightening the bolts and taking the specimen through an additional sweep of the temperature range, during which a further sequence of measurements was taken under conditions of temperature equilibrium. The results from these four runs are plotted in Fig. 5, from which it may be seen that they agree with one another within the limits of experimental uncertainty. A detailed consideration of the experimental uncertainties involved in measurements made with the Searle's bar system indicates that results taken with the electrolytic iron reference sample should be accurate to within ±3% at 80 K, rising to ±4% at 270 K. In the case of the composite bars containing HMS fibre, the figures are similar, while for the composite bars containing HTS fibre, the corresponding figures range between ±5% and ±7% at 80 K, to between ±7% and ±10% at 270 K.

In the case of the disc specimens it was necessary to correct for the thermal resistance of the layers of grease separating the blocks carrying the thermometers from the specimens. From a consideration of the thermal resistance of the sandwich consisting of a disc specimen flanked by layers of grease, it is not difficult to show that the thermal conductivity, K, of the specimen of thickness t_s is related to the thermal conductivity, K_g, of the grease layers, having an overall thickness t_g, by the equation

$$t_s = K\left(\frac{t_s}{K_m}\right) - K\left(\frac{t_g}{K_g}\right), \qquad (1)$$

in which K_m is the measured thermal conductivity of the sandwich. Measurements of values of K_m for discs of different thickness t_s clearly provide data for a graph of t_s against t_s/K_m, the slope of which should give the required thermal conductivity, K, of the specimens directly. Preliminary measurements indicated that the influence of small variations in t_g from one sample to another were sufficiently small to be discounted. This strength-

ened the basis upon which corrections were applied for the grease layers in subsequent measurements upon the discs, groups of between three and five of which were employed, having thicknesses ranging between approximately 1 and 5 mm. A detailed consideration of the experimental uncertainties in the case of the Lees' disc system yielded figures ranging between ±3% and ±10% over the temperature range of the measurements, the low temperature limit of which was limited by the viscosity of the grease.

4.2. Comparison with related work

The value of a comparison of the results of an investigation such as the present one with those of other workers is limited by the number of variables involved, although it does help to create a context within which a perspective may be gained in the long term. Perhaps the most relevant investigation for the present purpose is that of Knibbs *et al.* [10] with whose results the present thermal conductivities are compared in Figs. 6 to 8.

The temperature dependence of the thermal conductivity of the resin DX210/$BF_3$400, displayed in Fig. 6, contains no unusual features and an extrapolation of the results to the assumed temperature of the isolated result for epoxy resin MY750/DDM [10] indicates that these have similar magnitudes. The results for the present unidirectional specimen reinforced with HMS fibre, displayed in Fig. 7, extrapolate to a value similar to that of the corresponding result of Knibbs *et al.* [10], the fibre volume fraction of whose specimen was comparable, though the origin of whose fibres is not known. Combining this uncertainty with the known difference of identity of the resins, the comparison reveals nothing surprising. Similar remarks apply to a comparison of the corresponding results for unidirectional composites containing HTS fibre, displayed in Fig. 8.

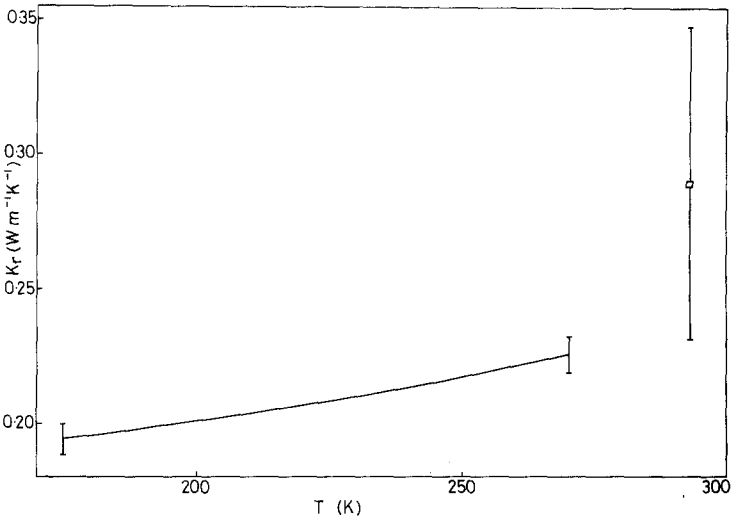

Figure 6 The thermal conductivity K_T of epoxy resins DX 210/$BF_3$400 and MY 750/DDM, in which the estimated uncertainties are indicated by the vertical lines: ⊢⊣ present results for specimens 1 (DX210/$BF_3$400), ⊢ the results of Knibbs *et al.* [10] for MY 750/DDM.

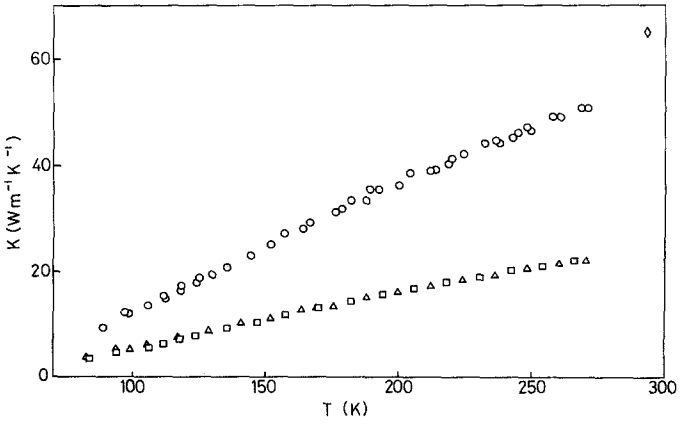

Figure 7 The thermal conductivities K of HMS carbon fibre-reinforced plastics: ○ present results for specimen 2; □ present results for specimen 4; △ present results for specimen 5; ◇ Knibbs *et al.* [10].

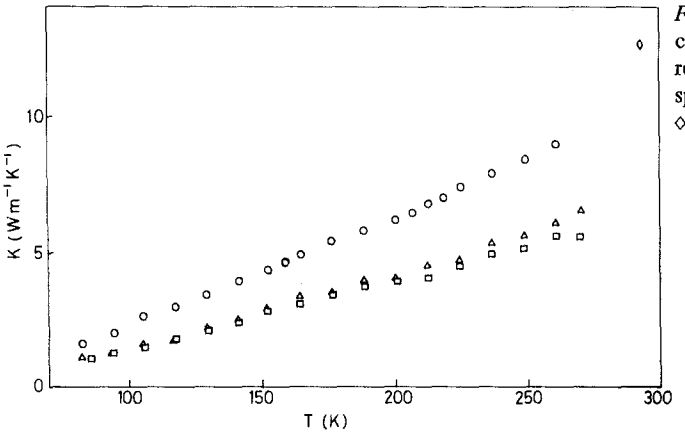

Figure 8 The thermal conductivities K of HTS carbon fibre-reinforced plastics: ○ present results for specimen 6; □ present results for specimen 10; △ present results for specimen 11; ◇ Knibbs *et al.* [10].

5. Discussion

5.1. Qualitative observations

A number of qualitative observations are possible:

(i) the thermal conductivity of the pure resin is the lowest of all the specimens examined;

(ii) the thermal conductivity in the fibre direction of the HMS carbon fibre unidirectionally reinforced plastic specimen 2 exceeds that of each of the corresponding 90° cross-plies, i.e. specimens 4 and 5, which in turn exceed that in the transverse direction of the corresponding unidirectionally reinforced specimen 3;

(iii) the thermal conductivities of the 0°–90° and ±45° HMS carbon fibre-reinforced plastic specimens 4 and 5 are identical, within the limits of experimental uncertainty;

(iv) the thermal conductivity in the fibre direction of the HTS carbon fibre unidirectionally reinforced plastic specimen 6 exceeds that of each of the corresponding 90° cross-plies, i.e. specimens 10 and 11, which in turn exceed that in the transverse direction of the corresponding unidirectionally reinforced specimen 8;

(v) the thermal conductivities of the 0°–90° and ±45° HTS carbon fibre-reinforced plastic specimens 10 and 11 are identical, within the limits of experimental uncertainty;

(vi) the thermal conductivity in the fibre direction of the HMS carbon fibre unidirectionally reinforced plastic specimen 2 exceeds that of the corresponding HTS fibre-reinforced specimen 6;

(vii) the thermal conductivities of the 90° cross-plied laminates containing HMS fibre, i.e. specimens 4 and 5, exceed that of the corresponding HTS fibre-reinforced specimens 10 and 11;

(viii) the thermal conductivities in the transverse direction of the HTS carbon fibre unidirectionally reinforced specimens 7, 8 and 9 increase with fibre volume fraction.

None of these observations conflict with expectation and the comparative observations involving the HMS and HTS fibres accord with the idea of the c-crystallographic axes of the graphite crystallites in the HMS fibres being more nearly at right angles to the fibre axis than those in the HTS fibres.

5.2. Analysis of data

5.2.1. The Searle's bar results

5.2.1.1. The longitudinal thermal conductivities of the carbon fibres. The thermal conductivity of a unidirectionally reinforced composite in a direction parallel to the fibres, K_{11}^{c}, may be expressed in terms of the corresponding conductivities of the fibres, $K_{\parallel}^{f}$, and the resin matrix, K_r, by the equation,

$$K_{11}^{c} = K_{\parallel}^{f} v_f + K_r (1 - v_f), \qquad (2)$$

in which v_f is the fibre volume fraction. Applying the results for specimens 1, 2 and 6 to this equation has permitted the calculation of the longitudinal conductivities, $K_{\parallel}^{f}$, of the fibres. These are illustrated in Fig. 9 together with the results of Volga *et al.* [11]. The orientation of the c-crystallographic axis of the graphite crystallites to the fibre axis, which has been indirectly shown to be related to their longitudinal thermal conductivity, may be expected to be directly related to the thermal history. Examination reveals two features which are common to both sets of results. The temperature dependence of the longitudinal thermal conductivity is similar in both cases and the absolute magnitude increases with graphitization temperature. Numerical differences

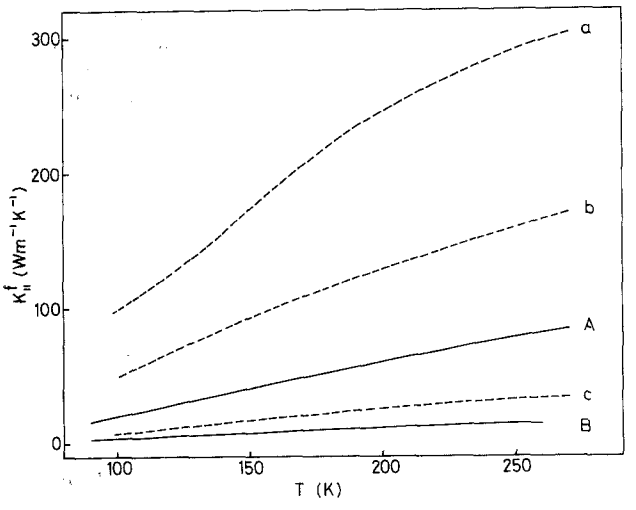

Figure 9 The longitudinal thermal conductivities $K_{\parallel}^{f}$ of carbon fibres expressed in smoothed form: A, present results for HMS fibre (approximate graphitization temperature 2600° C); B, present results for HTS fibre (approximate graphitization temperature 1500° C); a, b, c results of Volga *et al.* [11] for fibres heat-treated for 1 h at temperatures of 2800, 2600 and 1400° C, respectively.

between the two sets of results probably arise from differences in the production of the fibres.

5.2.1.2. The effect of fibre orientation. The basic transformation equation for the in-plane thermal conductivity of unidirectionally fibre-reinforced composites may be written in the form

$$K_{\theta}^{c} = K_{11}^{c} \cos^2\theta + K_{22}^{c} \sin^2\theta, \quad (3)$$

in which K_{θ}^{c} is the thermal conductivity of the composite in a direction inclined at an angle θ to the principal fibre direction and K_{22}^{c} is the value in the transverse direction, i.e. when $\theta = \pi/2$. Turning to the case of a bidirectional laminate consisting of n_1 laminae orientated at an angle θ to the direction of measurement and n_2 exactly similar laminae orientated at an angle ϕ, the contributions from the two laminae may be expressed in the terms of Equation 3 and then added to give the thermal conductivity

$$K_{\theta,\phi}^{c} = p_{\theta} (K_{11}^{c} \cos^2\theta + K_{22}^{c} \sin^2\theta) + p_{\phi} (K_{11}^{c} \cos^2\phi + K_{22}^{c} \sin^2\phi), \quad (4)$$

where $p_{\theta} = n_1/(n_1 + n_2)$ and $p_{\phi} = n_2/(n_1 + n_2)$ are called the packing fractions. All the bidirectional cases considered here were balanced, so that $p_{\theta} = p_{\phi} = 1/2$. In the cases of specimens 4 and 5 Equation 4 reduces to

$$K_{0,\pi/2}^{c} = K_{\pm\pi/4}^{c} = (K_{11}^{c} + K_{22}^{c})/2, \quad (5)$$

which are particular cases of the more general result

$$K_{\theta,\pi/2-\theta}^{c} = (K_{11}^{c} + K_{22}^{c})/2, \quad (6)$$

which follows directly from an addition of appropriate terms having the form of Equation 3 and illustrates the isotropy of the in-plane thermal conductivity of a balanced bidirectional laminate. The equality of the results for specimens 10 and 11 is to be expected for the same reason. Figs. 7 and 8 illustrate that the results for the bidirectional composites containing HMS and HTS fibres both conform with this expectation.

5.2.1.3. Calculation of composite conductivities. Pursuing the self consistency of the results beyond the establishment of equalities such as those considered above, Equation 5 permits the calculation of the in-plane thermal conductivities of the laminates in terms of the corresponding values for the appropriate laminae. The results of such calculations, after adjusting for differences of fibre volume fraction and packing fraction, are illustrated

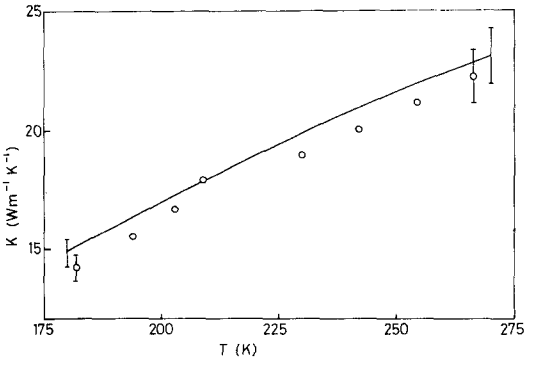

Figure 10 The thermal conductivity K of specimen 4, in which the estimated uncertainties are indicated by the vertical lines: ⊹ measured; ⊢⊣ calculated from the results for specimens 2 and 3.

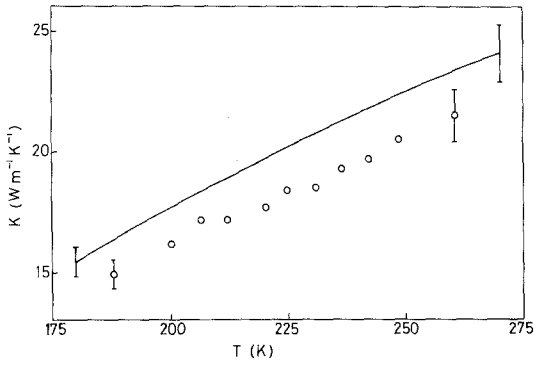

Figure 11 The thermal conductivity K of specimen 5, in which the estimated uncertainties are indicated by the vertical lines: ⊦ measured; ⊢⊣ calculated from the results for specimens 2 and 3.

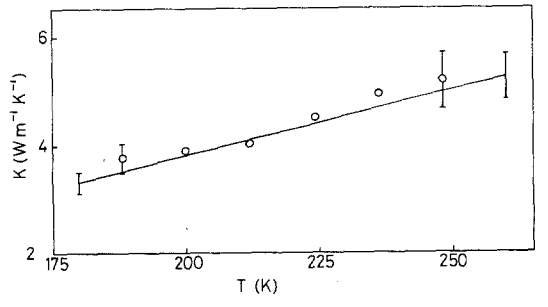

Figure 12 The thermal conductivity K of specimen 10, in which the estimated uncertainties are indicated by the vertical lines: ⊦ measured; ⊢⊣ calculated from the results for specimens 6 and 8.

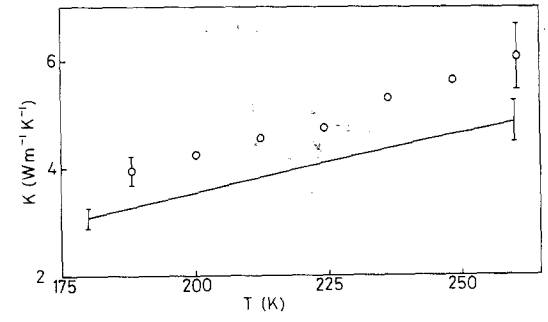

Figure 13 The thermal conductivity K of specimen 11, in which the estimated uncertainties are indicated by the vertical lines (see text): ⊦ measured; ⊢⊣ calculated from the results for specimens 6 and 8.

in Figs. 10 to 13. In the first three of these figures agreement between observation and calculation may be seen to be within the limits of experimental uncertainty. In the case of specimen 11 the agreement lies outside these limits. As explained in Section 2.3, practical considerations necessitated the fibre for specimen 11 being drawn from a different batch from that employed for specimens 6 and 10 and it seems likely that herein lies the cause of the outstanding difference.

5.2.2. The Lees' disc results

5.2.2.1. General. Various models have been put forward in an attempt to express the transverse thermal conductivity of a unidirectional composite in terms of the thermal conductivities of the matrix and the included fibres. Some of these are examined below, when the relative credibilities of the models will be assessed by the extent to which they provide a self consistent account of some of the experimental data.

5.2.2.2. The series electrical resistance analogy. Drawing an analogy with an electrical circuit in which the components are connected in series, Thornburgh and Pears [12] derived the equation

$$\frac{1}{K^c_{22}} = \frac{v_f}{K^f_\perp} + \frac{(1-v_f)}{K_r}, \tag{7}$$

in which $K^f_\perp$ is the thermal conductivity of the fibres in the transverse direction and the other terms have their previous meanings. Re-arranging the terms in this equation and assuming various values for the ratio $K_r/K^f_\perp$, a comparison with the results for specimens 7, 8 and 9 reveals an improving agreement with experiment as $K_r/K^f_\perp$ increases to infinity. However, even in this limiting case, agreement is poor and it is necessary to resort to a modified model in order to achieve improved agreement. Ignoring the influence of voids, the volume fractions of which are very low in the present cases, and making no allowance for direct fibre-to-fibre contact, the form of their modified equation adopted for the comparison illustrated in Fig. 14 was

$$K^c_{22} = BK_r(1-v_f) + \frac{[v_f + (1-B)(1-v_f)]\,K^f_\perp K_r}{[v_f K_r + (1-B)(1-v_f)K^f_\perp]}. \tag{8}$$

In this equation, B is the volume fraction of the resin which is assumed to present a continuous path for heat flow. A more sophisticated representation would involve taking account of a decrease of B which must accompany an increase of v_f, but for the present purpose a constant value of $B = 0.4$ was assumed. Within the limitations imposed by the available experimental data and

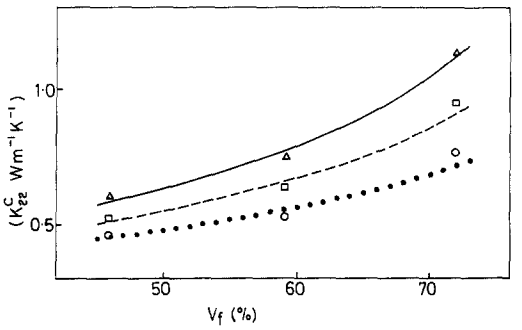

Figure 14 The transverse thermal conductivities K_{22}^c of the unidirectional composites reinforced with HTS fibre. Smoothed experimental results: ○, 180 K; □, 225 K, △, 270 K. Results calculated on the basis of the series electrical resistance analogy: ..... ($K_\perp^f = 1.7$ W m^{-1} K^{-1}), – – – ($K_\perp^f = 3.5$ W m^{-1} K^{-1}), ——— ($K_\perp^f = 10.0$ W m^{-1} K^{-1}).

assumptions, the agreement achieved by assuming values for $K_\perp^f$ of 1.7, 3.5 and 10.0 W m^{-1} K^{-1} at 180, 225 and 270 K, respectively, must be regarded as being reasonably favourable.

5.2.2.3. The in-plane shear field analogy. The shear stress distribution in a filamentary composite has been discussed in terms of a basic unit cell under the assumptions of a regular periodic array of parallel fibres, with both macroscopic homogeneity, local fibre isotropy and matrix isotropy, by Adams and Doner [13]. Springer and Tsai [14] showed that a series of transformations could be employed to develop an analogous treatment of transverse heat flow, in which displacement was replaced by temperature, the average shear stress was replaced by the average heat transfer rate and thermal conductivity replaced shear modulus. The treatment of Adams and Doner proved to be inconvenient for immediate application and a simpler analysis of thermal conduction in composites was achieved by transforming the Halpin–Tsai equations to the form:

$$\frac{K_{22}^c}{K_r} = \frac{1 + \zeta\eta v_f}{1 - \eta v_f} \tag{9}$$

in which

$$\eta = \frac{(K_\perp^f/K_r) - 1}{(K_\perp^f/K_r) + \zeta},$$

$$\ln \zeta = \sqrt{3} \ln\left(\frac{d}{t}\right),$$

and d/t was the aspect ratio of the fibres. Applying this treatment to the present results in a manner similar to that employed previously resulted in the comparison depicted in Fig. 15. The degree of agreement is comparable with that achieved with the earlier model, but this time the transverse thermal conductivity of the fibre came out to be 2.0, 3.1 and 5.7 W m^{-1} K^{-1} at 180, 225 and 270 K, respectively.

5.2.2.4. The axial shear loading analogy. Adopting a different approach to the problem through an essentially similar analogy, Hashin [15] derived predictive equations for upper and lower limits for K_{22}^c. Agreement between the experimental results and the upper limiting value involved assuming values for $K_\perp^f$ which were much lower than those assumed in Sections 5.2.2.2 and 5.2.2.3 and even then agreement was poor. Meanwhile the lower limiting value proved to be identical to that employed in Section 5.2.2.3.

5.2.2.5. The elastic moduli analogy. This model, developed by Nielsen [16], is essentially an extension of the previous models, in which account is taken of the shape and packing of the fibres, as well as an allowance being made for possible variations in fibre dispersion. In this case use is made of a modification of the Halpin–Tsai equations, which take the form:

$$\frac{K_{22}^c}{K_r} = \frac{1 + CDv_f}{1 - D\psi v_f}, \tag{10}$$

where $C = k_E - 1$, k_E being the generalized Einstein coefficient,

$$D = \frac{(K_\perp^f/K_r) - 1}{(K_\perp^f/K_r) + C}$$

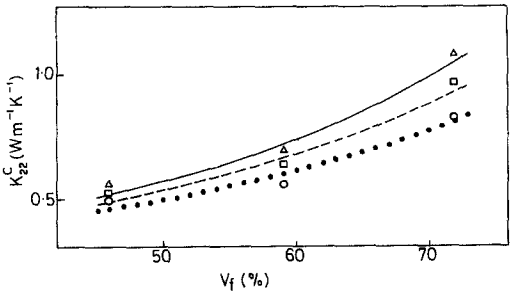

Figure 15 The transverse thermal conductivities K_{22}^c of the unidirectional composites reinforced with HTS fibre. Smoothed experimental results: ○, 180 K; □, 225 K; △, 270 K. Results calculated on the basis of the in-plane shear field analogy: ..... ($K_\perp^f = 2.0$ W m^{-1} K^{-1}), – – – ($K_\perp^f = 3.1$ W m^{-1} K^{-1}), ——— ($K_\perp^f = 5.7$ W m^{-1} K^{-1}).

$$\psi = 1 + \left(\frac{1 - v_m}{v_m^2}\right) v_f .$$

v_m is the maximum packing fraction for fibres in different packing schemes and the other terms have the same definitions as before.

Comparison with the in-plane shear field analogy reveals that D, like η, provides a measure of the relative conductivities of the two phases and C, like ζ, depends upon the shape and orientation of the fibres. v_m is defined as the ratio of the true volume of the dispersed phase to the volume it appears to occupy when at its maximum packing density and ψ allows for the type of fibre packing in the system. For an ideal lay-up of uniaxial fibres the appropriate value of C in the case of transverse heat flow is 0.5. However, Lewis and Nielsen [17] have shown that for composites containing fibres which are bunched, a value of $C = 0.84$ is more realistic. Adopting this value of C and assuming the typical value $K_\perp^f/K_r = 25$ from the earlier models, K_{22}^c/K_r has been evaluated at 270 K as a function of v_f for values of v_m corresponding to hexagonal (0.907), random (0.820) and square (0.785) packing, producing the results which are illustrated in Fig. 16. It is difficult to conclude from this figure whether hexagonal packing is favoured at all levels of fibre volume fraction examined or whether the form of fibre dispersion tends to adjust itself towards the hexagonal modification as the fibre volume fraction is increased. More experimental evidence is required in order to be able to discriminate between these possible packing modes.

5.2.2.6. The long waves model. Employing a method of analysis introduced earlier, Behrens [18] developed a model which involved calculations of the damping coefficients of thermal waves having wavelengths which were long compared with the inter-component spacing. Applying his treatment to the present situation finally led to an equation for K_{22}^c which was identical to the corresponding equation emerging from the in-plane shear field analogy.

5.2.2.7. The transverse thermal conductivity of carbon fibres. Analysis of the experimental composite results, obtained with the aid of the Lees' disc apparatus, provides the basis of assessments of the temperature dependence of the transverse thermal conductivity of the carbon fibres. The approximations and assumptions inherent in the models limit the reliance which may be placed upon any values derived with their aid. Likewise structural imperfections in the specimens and experimental uncertainties restrict the applicability of any theoretical models. Subject to these constraints, the results displayed in Fig. 17 have been derived employing the equation

$$K_\perp^f = \frac{K_r(1 - v_f) - K_{22}^c(1 + v_f)}{(K_{22}^c/K_r)(1 - v_f) - (1 + v_f)} . \quad (11)$$

This equation corresponds to the treatments based upon analogies in elasticity, with which a reasonable degree of agreement with experiment has been described. The small difference between the terms in the denominator prevents a realistic

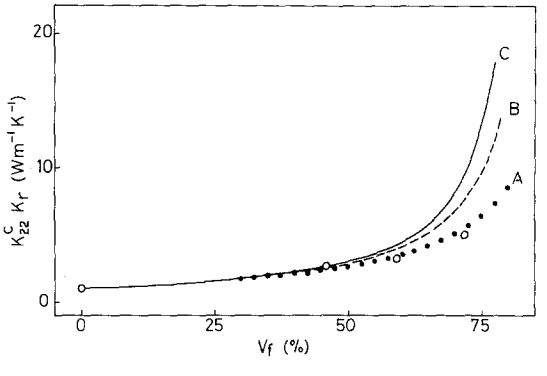

Figure 16 The reduced thermal conductivities K_{22}^c/K_r of specimens 1, 7, 8 and 9: ○ experimental data. Results calculated from Equation 10: ..... A (assuming hexagonal packing); — — — B (assuming random packing); ——— C (assuming square packing).

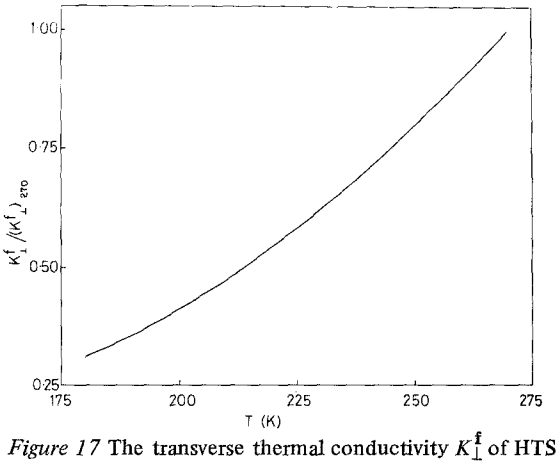

Figure 17 The transverse thermal conductivity $K_\perp^f$ of HTS fibre calculated from Equation 11 and expressed in reduced form, in which the value of $K_\perp^f$ at 270 K, i.e. $(K_\perp^f)_{270}$, was taken as 6.0 W m^{-1} K^{-1}.

assessment of $K_{\perp}^{f}$ in the case of HMS fibre and the values displayed for HTS fibre were based upon results for specimens 9, i.e. the specimens containing the highest fibre volume fraction, for which the uncertainty in the magnitude of the denominator of Equation 11 was least. The results are displayed in reduced form, in the derivation of which a value of $K_{\perp}^{f} = 6.0\,W\,m^{-1}\,K^{-1}$ was assumed at 270 K, in Fig. 17.

6. Conclusions

Reservations surrounding the application of idealized theories to interpretations of experimental data for physically imperfect materials inevitably qualify the value of deductions based upon them. In spite of this limitation, in addition to augmenting the relatively few data available for the thermal conductivity of carbon fibre-reinforced plastics and their constituents, the present experimental results have served to confirm a number of expectations based upon analytical treatments of thermal conduction in fibre-reinforced composites. A comprehensive appraisal of the standing of theoretical models must await the production of more nearly structurally perfect materials and improvements in experimental precision and accuracy. Meanwhile it may be concluded from the self consistency of the interpretations examined that the degree of understanding afforded by analogous treatments provides encouragement for the further parallel development of experimental and theoretical investigations in this field.

Acknowledgement

We wish to express our gratitude to the Science Research Council for a CAPS award received by one of us (M.W.P.).

References

1. R. B. PIPES, J. R. VINSON and TSU-WEI CHOU, *J. Comp. Mater.* **10** (1976) 129.
2. R. Y. KIM and J. M. WHITNEY, *ibid* **10** (1976) 149.
3. E. L. McKAGUE, J. D. REYNOLDS and J. E. HALKIAS, *Trans. ASME Ser. H* **98** (1976) 92.
4. C. H. SHEN and G. S. SPRINGER, *J. Comp. Mater.* **11** (1977) 2.
5. K. F. ROGERS, L. N. PHILLIPS, D. M. KINGSTON-LEE, B. YATES, M. J. OVERY, J. P. SARGENT and B. A. McCALLA, *J. Mater. Sci.* **12** (1977) 718.
6. B. YATES, M. J. OVERY, J. P. SARGENT, B. A. McCALLA, D. M. KINGSTON-LEE, L. N. PHILLIPS and K. F. ROGERS, *ibid* **13** (1978) 433.
7. A. GERMAN, Ph.D. Thesis, University of Salford (1976).
8. J. G. HUST and L. L. SPARKS, Data sheet for NBS SRM 734 (1971), Washington DC, USA.
9. E. H. RATCLIFFE, *Brit. J. Appl. Phys.* **10** (1959) 22.
10. R. H. KNIBBS, D. J. BAKER and G. RHODES, "The thermal and electrical properties of carbon fibre unidirectional reinforced epoxy composites", 26th Annual Technical Conference, Reinforced Plastics/Composites Division, The Society of the Plastics Industry Inc. (1971).
11. V. I. VOLGA, V. I. FROLOV and V. K. USOV, *Inorg. Mater.* **9** (1973) 643.
12. J. D. THORNBURGH and C. D. PEARS, ASME Paper 65-WA/HT-4 (1965).
13. D. F. ADAMS and D. R. DONER, *J. Comp. Mater.* **1** (1967) 4.
14. G. S. SPRINGER and S. W. TSAI, *ibid* **1** (1967) 166.
15. Z. HASHIN, NASA contractor report CR-1974 (1972).
16. L. E. NIELSEN, *Ind. Eng. Chem. Fundam.* **13** (1974) 17.
17. T. B. LEWIS and L. E. NIELSEN, *Trans. Soc. Rheol.* **12** (1968) 421.
18. E. BEHRENS, *J. Comp. Mater.* **2** (1968) 2.

Received 20 July and accepted 20 September 1979